Electromagnetic and Transport Considerations in Subpicosecond Photoconductive Switch Modeling

SAMIR M. EL-GHAZALY, MEMBER, IEEE, RAVINDRA P. JOSHI, AND ROBERT O. GRONDIN, SENIOR MEMBER, IEEE

Abstract—**It is now possible to use optoelectronic techniques to both generate and measure electrical waveforms with subpicosecond rise times. These rise times invalidate assumptions commonly made in developing equivalent circuit models for transmission lines and other simplifications commonly made in modeling conductivity. In this paper we discuss how a combination of direct finite-difference time-domain solutions of Maxwell's equations and Monte Carlo models of photocarrier transport can be used to avoid making these assumptions.**

I. Introduction

PHOTOCONDUCTIVE switching and electro-optic sampling provide a basis for generating and measuring electrical waveforms with subpicosecond rise times. A photoconductive switch is a simple structure, a gap in a microstrip line laid down on a photoconductive substrate, with a variety of uses [1]. The switch is activated by exciting the gap with a laser pulse of duration under 0.1 ps. As these short laser pulses are generated at a repetition rate ranging from 1 kHz to 100 MHz, they also can be used to repetitively sample the fields propagating down the line. This is done by placing an electro-optic material near the line, shining the optical pulses through this material, and measuring the polarization shift generated by the electric field associated with the line [2]–[6].

A commonly used analysis of such experiments was developed by Auston [7]. In Auston's approach, the photoconductive switch is modeled by a time-varying conductance connected in parallel with a capacitance. This switch is then inserted between two ideal, lossless transmission lines, one terminated by a source and the other by an impedance. The use of such a simple transmission line model is questionable for waveforms with subpicosecond rise times. While more complicated equivalent circuits, incorporating transmission lines with frequency-dependent characteristic impedances, have been used [8], these models are not well suited for the present case. Instead, direct solutions of Maxwell's equations are needed for a more general and exact approach.

Maxwell's equations, however, do not provide a complete mathematical description of the problem. They must be supplemented by a set of constitutive relations. The problem considered here involves the interaction between an electromagnetic wave and photogenerated carriers. The carriers appear in Maxwell's equations as sources of electromagnetic fields. On the other hand, the fields are the forcing functions in the constitutive carrier transport model. A model of the interaction between these two systems can be accurate for subpicosecond rise times only if the models of both systems are accurate for subpicosecond rise times. Here, we use ensemble Monte Carlo (EMC) techniques to model the photoconductive response of the gap and direct solutions of Maxwell's equations to model the electromagnetics of the problem.

Switching transient problems can be solved either in the time domain or, for linear systems, in the frequency domain (by transforming the results into the time domain [9], [10]). The electromagnetic aspects of this problem are linear and can be investigated using such approaches. However, the photocarrier transport processes are highly nonlinear, thereby eliminating any frequency-domain approach to their modeling. Fortunately the time of interest to us is at most a few tens of picoseconds; therefore a direct time-domain solution of Maxwell's equations in conjunction with a Monte Carlo trasnport model is possible for this problem.

II. Transient Photoconductivity in Gallium Arsenide

In Fig. 1 we show the energy flows of importance in photoconductivity. An optical pulse is used to pump energy into the semiconductor by the generation of electron–hole pairs. In Fig. 2 we illustrate the possible pair generation processes in gallium arsenide. We can photogenerate electrons out of three different valence bands: the heavy hole band, the light hole band, and the split-off

Manuscript received August 21, 1989; revised November 28, 1989. This work was supported by the Air Force Office of Scientific Research, by the FGIA Program at Arizona State University, and by the National Science Foundation.

The authors are with the Center for Solid State Electronics Research, Arizona State University, Tempe, AZ 85287.

IEEE Log Number 9034819.

0018-9480/90/0500-0629$01.00 ©1990 IEEE

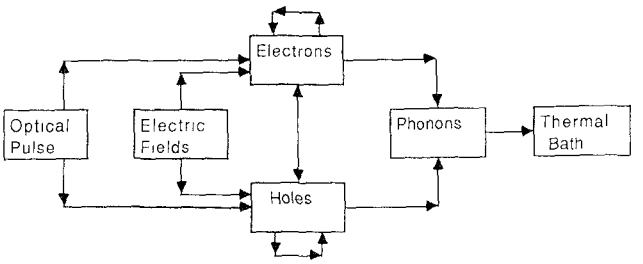

Fig. 1. Energy flow in photoconductivity.

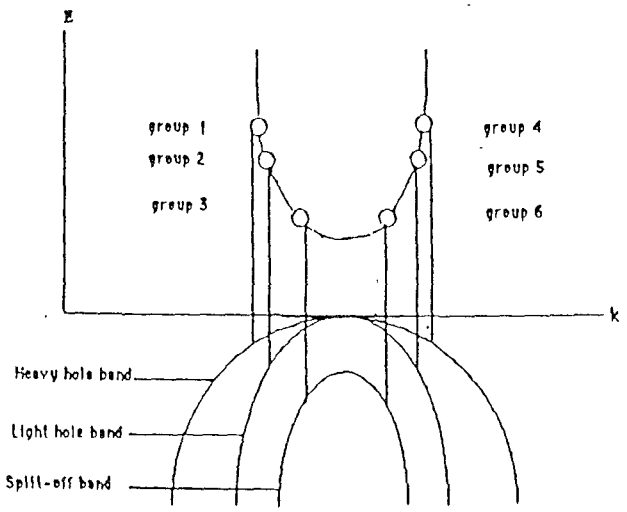

Fig. 2. Possible electron–hole pair generation in GaAs.

band, provided that the photon energy is sufficient for any individual transition. As is shown in Fig. 2, the photogeneration process is as likely to produce an electron with a negative velocity as it is an electron with a positive velocity. Therefore, the initial photocurrent is zero. These carriers are accelerated by the electromagnetic fields present in our structure. As the average velocity or current builds, energy begins to flow from these fields into the carriers. Energy gained by the carriers flows out along several different paths. There are several different carrier–carrier interactions or scattering processes: the electron–electron interaction, hole–hole scattering, and electron–hole scattering. The first two merely reshuffle the energy (and momentum) inside one of the two carrier gases. The last, however, is of some importance. Due to the large difference in effective mass between electrons and holes, there is a net flow of energy from the electron gas into the hole gas [11]. Both carrier species also lose energy to the crystal lattice through the process of optical phonon emission. Since they emit optical phonons at rates in excess of the absorption rate, the population of the optical phonon modes is driven up to levels above their equilibrium values. As this goes on, the absorption rate, which is proportional to the number of phonons available for a carrier to absorb, increases. The emission rate, however, remains constant and therefore the net rate at which energy flows from the carriers to the lattice decreases. It takes several picoseconds, however, for this hot phonon effect to build [12]. Eventually, these phonons decay back to their equilibrium levels and the system is thus connected to a heat bath.

The assumption effectively made by Auston, and used in other models of photoconductivity as well [13], [14], is that the system instantaneously achieves a steady state. Under this assumed situation, the rate at which the carriers gain energy from the fields is equal to the rate at which they lose energy to the bath. We will refer to such models as being quasi-static. However, such a steady state takes several picoseconds to be established following the incidence of a short laser pulse. In Fig. 3 we illustrate this by an EMC calculation of the average electron velocity following photogeneration into GaAs. If a quasi-static model were used, the carriers would be assumed to instantaneously reach their final steady-state velocity. As can be seen, this is a poor approximation.

Transient responses for photoexcitation into GaAs, such as that of Fig. 3, are wavelength dependent. When the optical wavelength is long enough, no electrons are generated near or above the energy threshold for intervalley scattering. For sufficiently short wavelengths, however, electrons are photogenerated above this threshold. Several things then happen. First, many of these electrons rapidly scatter to the higher mass valleys and the initial transients, especially at low electric fields, are dominated by a gradual return over several picoseconds of these electrons to the central valley. Additionally, for higher fields, there is a preferential selection of negative-velocity electrons as survivors in the central valley. Such electrons lose energy to the field and thereby fall below the intervalley scattering threshold. In summary, the photoresponse is not only wavelength dependent but also highly nonlinear and strongly affected by details of the electronic distribution in the energy bands [8].

The above results were calculated by the EMC technique, which we will generally use throughout this paper. This is one variation among many possible transport models. EMC calculations operate at the semiclassical level, where electrons are classical particles whose dynamics are controlled by the energy bands of the system and the various scattering processes are independent and instantaneous. While fully quantum mechanical models for transport exist [15], [16], they use different simplifying approximations. In an EMC simulation, we keep track of several thousand particles, accelerating them by the fields and statistically simulating the various individual scattering mechanisms. This is a computationally intensive task but it involves no assumptions beyond those made in the computation of the energy bands and scattering rates, assumptions which are shared by all semiclassical transport models. The Boltzmann transport equation is also computationally intensive, as it is a nonlinear, integrodifferential equation while its accuracy is limited by its use of a single time distribution function [17].

Simpler models [18], [19] model only the average flow of energy and momentum through the system without assuming the existence of a steady state. These models cannot describe the preferential selection of negative-

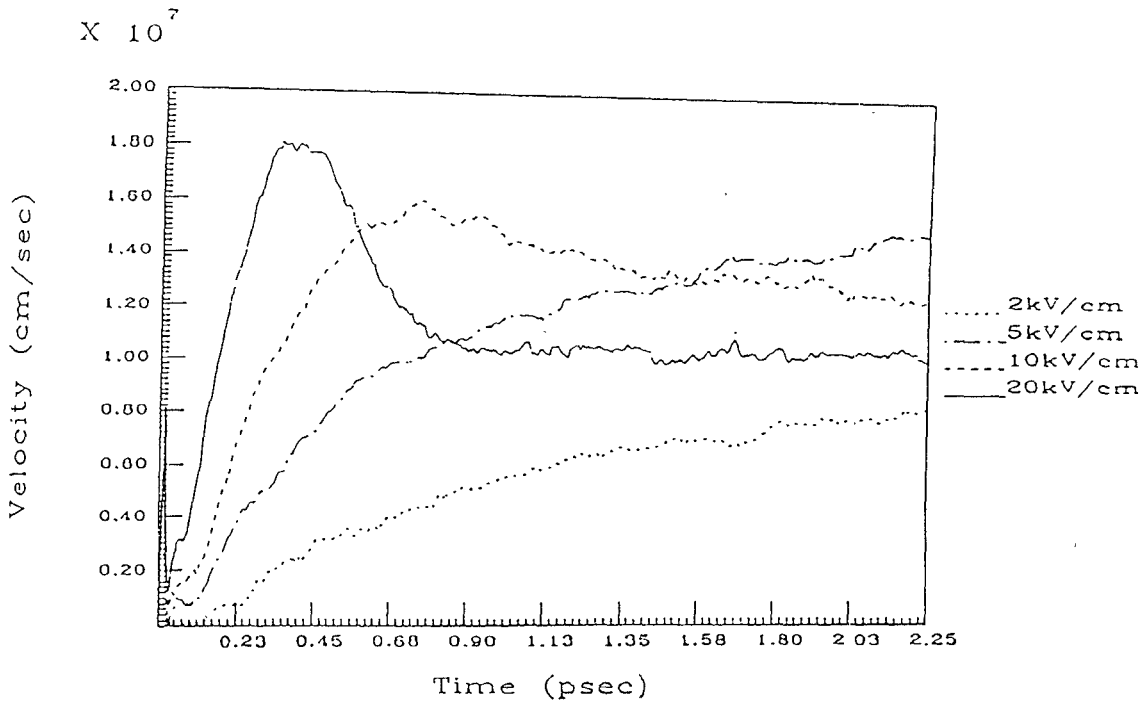

Fig. 3. Average electron velocity calculated using EMC.

velocity electrons as survivors in the central valley as they assume a specified shape to the distribution function [19]. In general, this assumed distribution function shape can lead to an inaccurate emphasis on the wrong energy-dependent scattering mechanism. Finally, we encounter the quasi-static models in which we assume that carriers instantaneously achieve a steady state with the field.

III. Electromagnetic Theory

Several techniques exist for solving Maxwell's equations in the time domain, including the transmission-line matrix method [20], the time-domain method of lines [21], and the finite difference method [22], [23]. Of these, the finite difference scheme is more convenient for this study since it directly discretizes the electric and magnetic fields using a rectangular mesh in space and decouples the fields over a small time interval (Δt). Therefore, the spatial and temporal characteristics of the fields can easily be visualized and incorporated inside the semiconductor model.

Maxwell's equations can be reduced to three independent equations in the unknowns: $\boldsymbol{E}$, the electric field; $\boldsymbol{B}$, the magnetic flux density; $\boldsymbol{H}$, the magnetic field; $\boldsymbol{D}$, the electric flux density; $\boldsymbol{J}$, the conduction current density; and Q, the total electric charge density. They must be supplemented by constitutive relations. Here we assume a uniform, linear, isotropic medium for the dielectric and magnetic relations and use the EMC for the conductivity model. The quantities ϵ and μ are the permittivity and permeability of the medium respectively. Hence, the electromagnetic wave propagation in this medium can be completely characterized by just solving the equations

$$\nabla \times \boldsymbol{E} = -\mu \frac{\partial \boldsymbol{H}}{\partial t} \tag{1a}$$

$$\nabla \times \boldsymbol{H} = \epsilon \frac{\partial \boldsymbol{E}}{\partial t} + \boldsymbol{J} \tag{1b}$$

$$\nabla \cdot \boldsymbol{J} = -\frac{\partial Q}{\partial t}. \tag{1c}$$

These are three equations in three unknowns, (i.e., $\boldsymbol{E}$, $\boldsymbol{H}$, and $\boldsymbol{J}$), while Q is considered a source. In an ideal dielectric medium, where $\boldsymbol{J}$ and Q are zeros, (1a) and (1b) are sufficient to describe the electromagnetic phenomena. The details of the solution in the pure dielectric structure can be found elsewhere [22], [24].

We assume that the semiconductor has a uniform, linear, isotropic dielectric constant and replace (1a) by the three scalar equations

$$\frac{\partial E_z}{\partial y} - \frac{\partial E_y}{\partial z} = -\mu \frac{H_x}{\partial t} \tag{2a}$$

$$\frac{\partial E_x}{\partial z} - \frac{\partial E_z}{\partial x} = -\mu \frac{\partial H_y}{\partial t} \tag{2b}$$

and

$$\frac{\partial E_y}{\partial x} - \frac{\partial E_x}{\partial y} = -\mu \frac{\partial H_z}{\partial t}. \tag{2c}$$

There are three similar equations that correspond to (1b). Discretizing the electric field over a three-dimensional

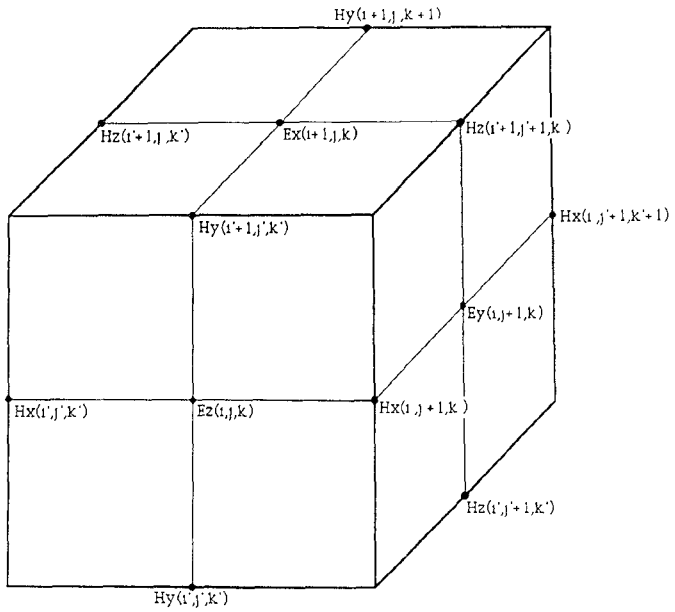

Fig. 4. The rectangular mesh used in discretizing Maxwell's equations.

spatial mesh as shown in Fig. 4, (2a) becomes

$$\frac{E_z^t(i,j,k)-E_z^t(i,j-1,k)}{\Delta y} - \frac{E_y^t(i,j,k)-E_y^t(i,j,k-1)}{\Delta z} = -\mu\frac{H_x^{t'+\Delta t}(i',j',k')-H_x^{t'}(i',j',k')}{\Delta t}. \quad (3)$$

Similar difference equations exist for (2b) and (2c).

For the magnetic field, a similar set of equations can be developed over a three-dimensional spatial mesh (i',j',k') and time (t'). One should notice that the electric field mesh (i,j,k) and time (t) are displaced from the magnetic field mesh (i',j',k') and time (t') by half the mesh increments (Δx, Δy, Δz, and Δt), as shown in Fig. 4, to achieve the proper definition of fields in space and time.

These equations are written in a matrix form as follows:

$$\boldsymbol{H}_x^{t'+\Delta t} = \boldsymbol{H}_x^{t'} + A_1\boldsymbol{E}_z^t + A_2\boldsymbol{E}_y^t \quad (4a)$$

$$\boldsymbol{H}_y^{t'+\Delta t} = \boldsymbol{H}_y^{t'} + A_3\boldsymbol{E}_x^t + A_4\boldsymbol{E}_z^t \quad (4b)$$

$$\boldsymbol{H}_z^{t'+\Delta t} = \boldsymbol{H}_z^{t'} + A_5\boldsymbol{E}_y^t + A_6\boldsymbol{E}_x^t \quad (4c)$$

where $\boldsymbol{H}_x^{t'+\Delta t}, \boldsymbol{H}_x^{t'}, \boldsymbol{E}_z^t, \boldsymbol{E}_y^t$, etc., are vectors containing the numerical values of the fields at the different time intervals, and A_1, A_2, etc., are matrices containing the information about the structure, the mesh, and the boundary conditions. There are three similar equations for the electric field components at time $t+\Delta t$. The time evolution scheme is shown in Fig. 5. The time dependence of the current density, $\boldsymbol{J}$, is discussed in Section V.

Our switching transient starts from an initial self-consistent distribution of the fields and charges. If the device is not biased and contains no free charges, then it may be assumed that the initial fields are zero. However,

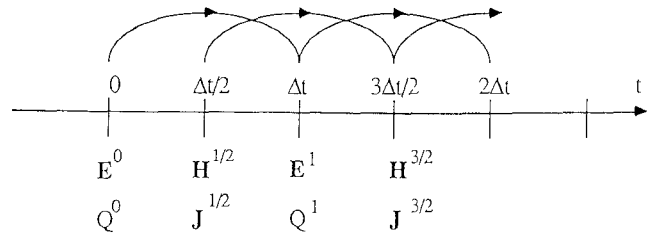

Fig. 5. The evolution scheme.

when the device is biased, one should initially solve for the dc charges and currents which are the sources for the electric and magnetic fields. Then, the fields can be obtained from their sources by using a suitable set of equations.

Our problem also has boundaries on which the tangential electric and magnetic fields must be known. In practical cases, the semiconductor device is surrounded by either metallic surfaces or open space (i.e., air). The metallic conductors are normally approximated as perfect conductors, which leads to zero tangential electric fields. For the open space boundaries, no such direct physical scheme exists. Therefore, one may enclose the structure inside a box of perfectly conducting electric or magnetic walls, selected based on the physics of the problem at hand and the degree of accuracy required, as we will do here. The alternative solution is to use absorbing boundary conditions to artificially simulate open space [25], [26].

IV. The Monte Carlo Approach

We shall briefly outline here the main features of our EMC algorithm, which has been used to study the transient transport of the photoexcited carriers. Creation of the electron–hole pairs is simulated by adding particles according to the line shape of the laser pulse. A three-valley electron and three-band hole model under the effective mass approximation is used for determining the initial energy and wave vector distribution. The starting k-space distribution is assumed to be isotropic, thus neglecting any effects of warped hole bands and polarized laser pulses [27]. By varying the initial energy assigned to the photogenerated carriers. we can simulate an arbitrary laser wavelength. The carrier photogeneration monotonically decreases with depth according to a decaying exponential with the decay set by α, the optical absorption coefficient.

The present bipolar EMC includes all the relevant carrier–phonon and carrier–carrier scattering mechanisms. Single-mode LO and TO couplings via the polar and optical deformation potential have been used, while all plasmon–phonon interactions have been ignored. Nonpolar acoustic scattering has also been included for completeness since it is momentum randomizing in nature and affects the carrier drift velocity. The calculations of the carrier scattering rates and the choice of the scattering mechanisms are made according to techniques outlined by Jacoboni and Reggiani [28]. A static but time evolving screening model proposed by Osman and Ferry

[29] is used for the polar interactions. Under this scheme, the time changing distributions and carrier energies are used to update the effective screening length. The main contribution to the screening process under this static model comes from the low-energy heavy holes.

Carrier–carrier scattering is also an important process and has been incorporated into the present EMC simulations. The electron–hole scattering affects the ultrafast transient behavior by providing an additional channel for energy transfer [30]. This energy loss is dominant for carriers having energy below the phonon emission threshold, and can even become important at higher carrier energies for densities exceeding 5×10^{17} cm^{-3} [11]. Electron–electron and hole–hole collisions have been left out since they do not change the ensemble momentum and energy of each carrier type.

V. Coupling the Time-Varying Electromagnetic Fields with the EMC Method

The EMC is a semiclassical approach for describing the response of individual particles to external driving forces. On the other hand, electromagnetic fields obtained from a solution of Maxwell's equations are based on a fluid model. In order to create the link between the common physical parameters of the kinetic EMC and the fluid electromagnetic model, we use the following scheme.

From the EMC point of view, space is divided into cubic cells. The electric and magnetic fields influencing the carrier motion are considered uniform within each cell. The carriers are positioned within the cell according to the initial distribution. As was described in Section III, the electric and magnetic fields obtained from the finite difference scheme are defined on the boundaries of the mesh used for the electromagnetic calculations. The cell used for the EMC, however, does not coincide with the three-dimensional mesh used in the electromagnetic solution. Therefore, the electric and magnetic fields resulting from the finite difference scheme have to be converted before being passed to the EMC program.

The current density distribution represents the feedback element from the EMC program for updating the electromagnetic fields. Therefore, some conversion is required from the EMC particle definition of the current to the electromagnetic fluid definition of the current density. The current densities are defined in the center of the EMC cell; hence it is defined at the corner of the spatially shifted finite difference mesh. The current density is mathematically calculated as

$$\boldsymbol{J}(i,j,k) = \frac{q}{\Delta x\,\Delta y\,\Delta z}\left(\sum_{n=1}^{N^h(i,j,k)} S^h(i,j,k,n)V^h(i,j,k,n) - \sum_{n=1}^{N^e(i,j,k)} S^e(i,j,k,n)V^e(i,j,k,n)\right) \quad (5)$$

where $S^{h,e}$ and $V^{h,e}$ are, respectively, the supercharges and velocities associated with the holes and electrons within the (i,j,k)th cell, $N^{h,e}$ are the numbers of holes and electrons in the (i,j,k)th cell respectively, and Δx, Δy, and Δz are the mesh spacings in the three directions. These supercharges play an important role. They are required because while we can simulate only a few tens of thousands of particles, millions are present in the real device; therefore, each simulated particle corresponds to many real particles. By adjusting these supercharges on the fly, it is possible to introduce generation and recombination effects into the simulation.

We now outline the actual simulation process:

Step 0) The entire simulation begins by solving for the initial electric and magnetic field distributions before introducing the carriers. The initial distribution of the optically generated electron–hole pairs is calculated via the EMC scheme. The photogenerated carriers are allowed to drift under the influence of the initial fields for a period of $\Delta t/2$ starting from the $t=0$ instant. The current density distributions at $t=\Delta t/2$ are calculated using (5).

Step 1) The electric field, which is effectively defined at $N\Delta t$, is updated. The new electric field is used to update the magnetic field, which is effectively defined at $(N+1/2)\Delta t$, using (4).

Step 2) The carriers are allowed to drift, for a period of Δt, using the electric field obtained in step 1 and the magnetic field, effectively defined at $t=N\Delta t$, which is calculated as

$$\boldsymbol{H}^{N\Delta t} = 0.5(\boldsymbol{H}^{(N-0.5)\Delta t} + \boldsymbol{H}^{(N+0.5)\Delta t}). \quad (6)$$

At the end of this time step Δt, the current density distribution defined at $(N+1/2)\Delta t$ is calculated using (5).

Steps 1 and 2 are repeated until the entire period of interest is covered. These steps are summarized in the flowchart shown in Fig. 6.

VI. Results and Discussion

For demonstration purposes we simulate the structure shown in Fig. 7. This structure is a coupled microstrip line using undoped GaAs as the substrate. The thickness of the dielectric material, L_x, is 4.5 μm. The width of each strip, w_s, is 2 μm, and the separation between them, S, is 4 μm. One of the strips is grounded at both ends. The other strip has a gap, L_g, of width 5 μm with one end grounded and the other connected to a dc source of 8 V. This entire structure is enclosed within a metallic box of dimensions $L_x=7$ μm, $L_y=14$ μm, and $L_z=120$ μm. The entire space inside this metallic box is discretized using a three-dimensional uniform mesh with $\Delta x=\Delta y=\Delta z=0.5$ μm.

The laser pulse, of energy 1.55 eV and duration 30 fs (FWHM), is applied on the gap of width L_g mentioned above. Furthermore, we assume that this pulse uniformly covers the entire gap. The carrier concentration gener-

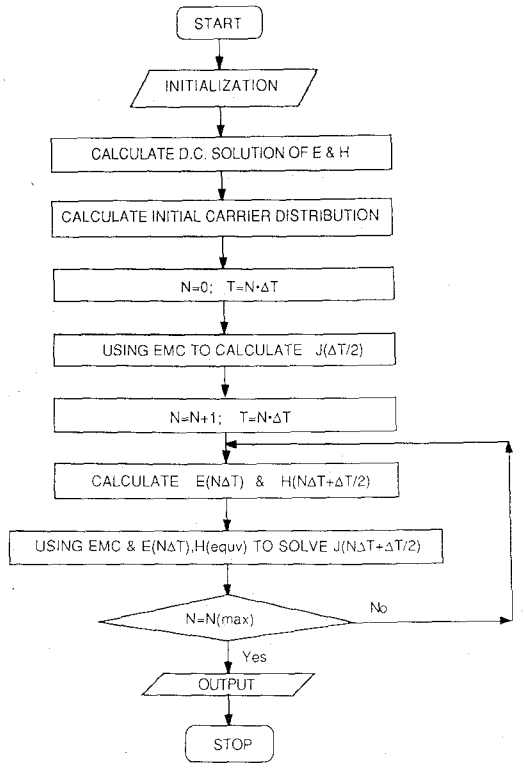

Fig. 6. The flowchart.

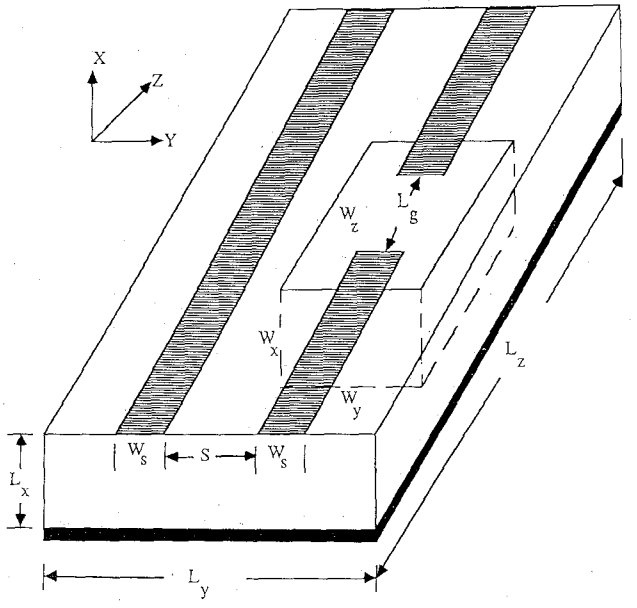

Fig. 7. The simulated structure and the EMC box.

ated by this pulse is taken to be 3×10^{16} cm^{-3}. Since undoped GaAs is used as the substrate, the thermally generated carriers at 300 K are negligible in comparison with the optically generated carriers. Based on this assumption, virtually no current flows prior to the application of the laser pulse.

The generated carriers are mainly concentrated around the gap. The carrier velocities in GaAs are typically of the order of 10^7 cm/s, so during the simulation times of interest here, the carriers drift only short distances away

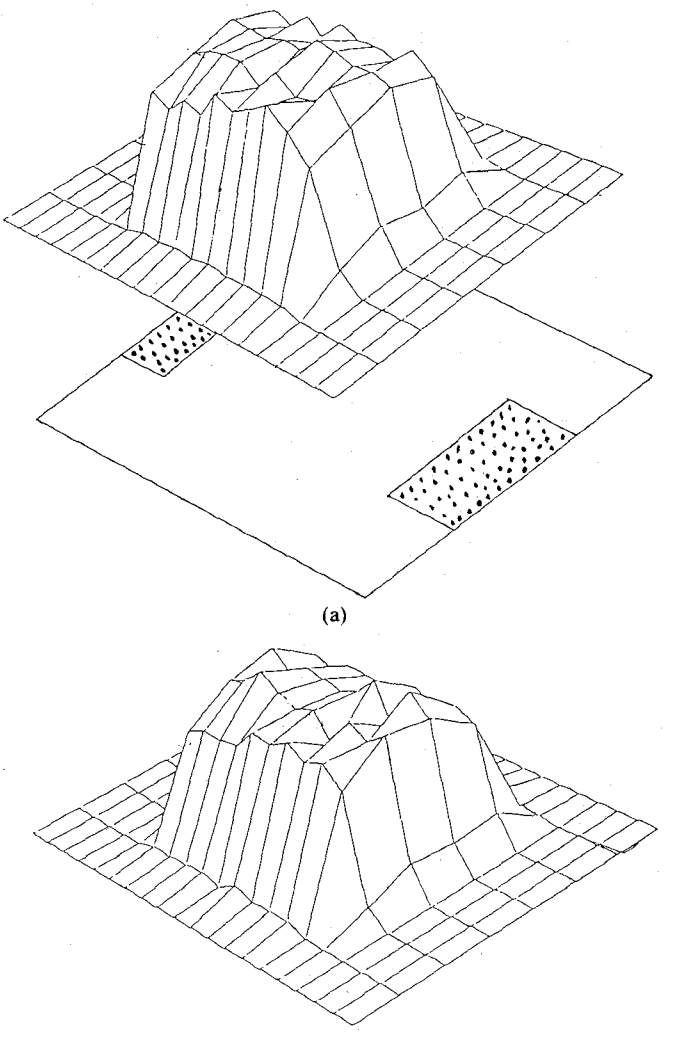

Fig. 8. The electron distribution in the cells below the air/GaAs interface at (a) $t = 0.3$ ps and (b) $t = 0.8$ ps.

from the gap. It is therefore reasonable to run the EMC only within the regions having mobile carriers, which, in this case, is the box of dimensions w_x, w_y, and w_z surrounding the gap as shown in Fig. 7. The results shown here are for $w_x = 2.5$ μm, $w_y = 4$ μm, and $w_z = 10$ μm. The metallic contacts absorb all incident mobile charge, and also supply the semiconductor with free carriers to maintain current continuity. Following a particle absorption process by the metal on one side of the gap, carriers are reinjected from the strip on the opposite side of the gap. The velocity of the reinjected particle is chosen randomly from a thermalized Maxwellian distribution. Other boundaries are assumed to have negligible surface recombination and are modeled as perfectly reflecting boundaries. Finally, 9000 electrons and holes are used to simulate the photogenerated carriers.

The electron density distributions in the cells immediately below the air/GaAs interface are shown in parts (a) and (b) of Fig. 8 0.3 and 0.8 ps after applying the laser pulse, respectively. Only a minor change in the electron distribution can be observed for the following reasons. First, the time span between the two distributions is

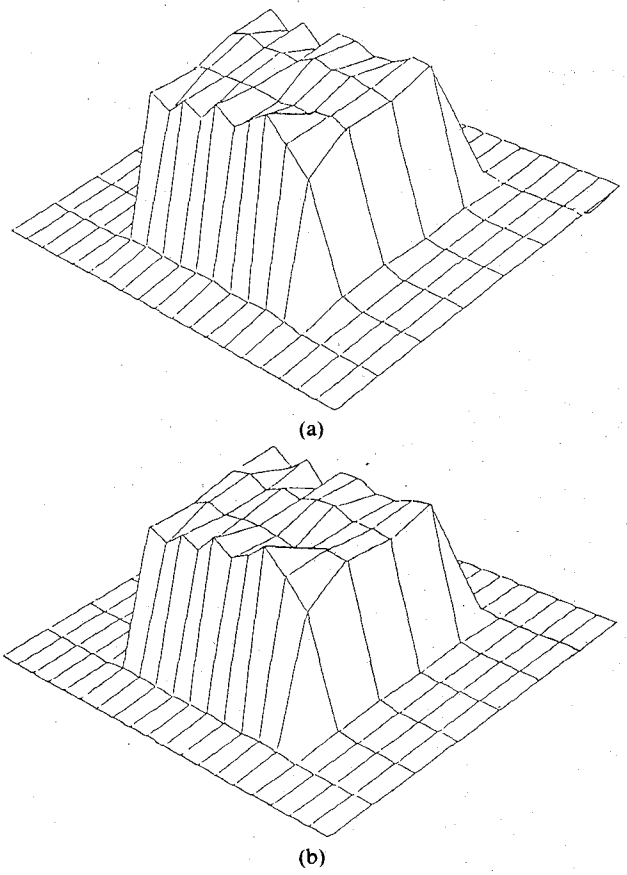

Fig. 9. The hole distribution in the cells below the air/GaAs interface at (a) $t = 0.3$ ps and (b) $t = 0.8$ ps.

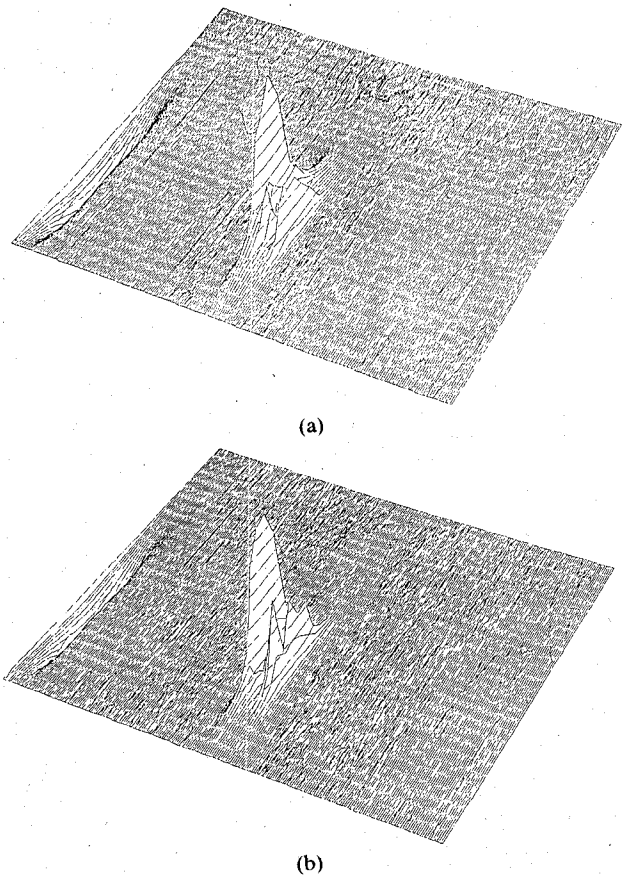

Fig. 10. E_z at the surface at (a) $t = 0.3$ ps and (b) $t = 0.8$ ps.

small, which means that the electrons could move only very short distances. This obviously would be altered by recombination in many situations. The last factor which can alter this has to do with the contacts. Contacts of the p type, for example, in a p-i-n structure cannot inject electrons. Here, since the electrons collected at one end were reinjected at the other, this effect has a minimal change on the distribution. However, the electron distribution spreading away from the gap, in the y direction, is noticeable. The hole distributions in the same cells at the same times are shown in parts (a) and (b) of Fig. 9. The change in this distribution is even smaller than that observed in Fig. 9. Obviously, this is due to the lower hole mobility.

The Z components of the electric field over the entire air/GaAs interface at $t = 0.3$ and 0.8 ps are shown in parts (a) and (b) of Fig. 10 respectively. Contrary to the electron and hole distributions, a significant change is observed in E_z. This is understood by knowing that even when the carrier distributions do not change, their velocity in the Z direction must dramatically increase; of course, this is up to a certain limit. However, the currents generated by the movement of carriers induce fields that oppose the original accelerating fields. This reduces the magnitude of the electric field in the gap. One should notice that the initial E_z in the gap (i.e., at $t = 0.0$) is not uniform, as was previously mentioned by Lu *et al.* [32].

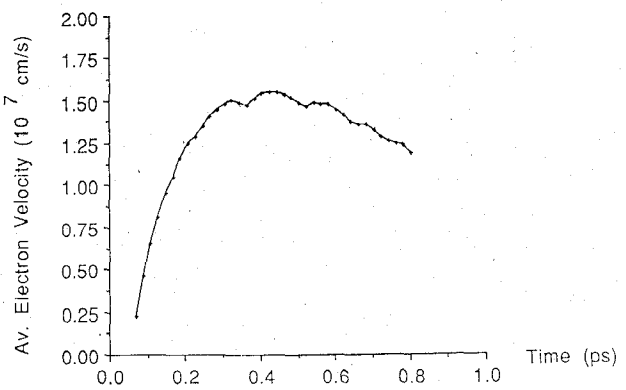

Fig. 11. The average electron velocity evolution with time.

The average electron velocity as a function of time is shown in Fig. 11. This velocity increases almost linearly with time for $t < 0.2$ ps. It reaches a maximum velocity that is slightly higher than 1.5×10^7 cm/s at about 0.5 ps and then decreases toward the expected saturation value of about 10^7 cm/s. This shape generally resembles the profiles seen in Monte Carlo simulations of photogeneration in spatially uniform, temporally constant fields.

There are several unresolved modeling issues. We already have referred to the question of how one models the open spaces seen in the real systems. We initially used a reflecting electric or magnetic wall, which introduces spurious reflections. While we might imagine the use of well-established boundaries as being useful in certain

precision measurements, we are equally sure that the vast majority of applications of photoconductive switching and electro-optic sampling will not involve placing the system in a metallic box. Therefore, the use of absorbing boundaries at the open edges is required. To exploit this interesting approach, we believe that some techniques must be used to reduce the computational effort (e.g., using a nonuniform mesh in the finite difference scheme) or to eliminate stability constraints on time step selection (by use of implicit numerical algorithms).

There also are boundary condition issues faced in the EMC. Since it is a particle-based simulation, you must ask what happens when the carrier hits the edge of the system being simulated. Generally, the edge either reflects it or absorbs it. If it is absorbed, then one must determine whether or not it is to be reinjected into the system and, if so, where and with what velocity. We have performed some investigations of this point [31] in which we again use flexible supercharges to better match the particle model with basic conservation rules.

There are also two material parameter issues not yet resolved. First, the dielectric constant of GaAs and other compound semiconductors is not constant over the wide frequency range needed for accurate modeling of such short rise times. In a time-domain simulation, we cannot directly employ a frequency-dependent constant. While we may be able to use the Monte Carlo to simulate the electronic contribution inside the gap, outside the gap this cannot be done. One approach would be to transform the frequency-dependent dielectric relation into a convolution integral in the time domain. Beyond introducing extra numerical problems, it complicates the transformation of (1b) to (2b).

The second material parameter issue is the electro-optic sampler. These materials do not have a simple, constant dielectric property but instead exhibit visible anisotropy. This, however, can be implemented relatively easily here. If this is done, we can then employ the code to determine the degree to which the introduction of an external electro-optic sampler changes the fields being sampled by it. A point of interest here is that the electro-optically induced polarization shift in the optical probe pulse is calibrated against dc line voltages. Raw data are generally presented then as a "line voltage" even though it is the electric field that is sensed. The relationship between the transient fields actually present and this transient line voltage is a primary target for future investigation.

VII. Conclusion

In summary, we have discussed a variety of problems that complicate the development of an accurate model for subpicosecond optoelectronic switching and the measurement of electrical waveforms on microstrip lines. We have also shown that the situation is certainly not hopeless by demonstrating that Monte Carlo techniques for modeling ultrafast carrier transport can be implemented in self-consistent fashion with a direct time-domain solution of Maxwell's equations, thus providing a model which makes relatively few assumptions.

Acknowledgment

The authors thank G. Mourou, K. Meyer, T. Norris and D. Ferry for useful conversations on this topic.

References

[1] D. H. Auston in *Ultrafast Laser Pulses and Applications*, W. Kaiser, Ed. Berlin: Springer-Verlag, 1988.

[2] J. A. Valdmanis, G. A. Mourou, and C. W. Gabel, "Subpicosecond electrical sampling," *IEEE J. Quantum Electron.*, vol. QE-19, pp. 664–667, Apr. 1983.

[3] K. E. Meyer and G. A. Mourou, "Two dimensional *E*-field mapping with subpicosecond resolution," in *Picosecond Electronics and Optoelectronics*, G. A. Mourou, D. M. Bloom, and C.-H. Lee, Eds. Berlin: Springer-Verlag, 1985.

[4] J. A. Valdmanis and S. S. Pei, "A non-contact electro-optic prober for high speed integrated circuits," in *Picosecond Optoelectronics and Optoelectronics* vol. II, F. J. Leonberger, C. H. Lee, F Capasso, and H Morkoc, Eds. Berlin: Springer-Verlag, 1987.

[5] B. H. Kolner, K. J. Weingarter, M. J. W. Rodwell, and D. M. Bloom, "Picosecond electrooptic sampling and harmonic mixing in GaAs," in *Picosecond Electronics and Optoelectronics*, G. A. Mourou, D. M. Bloom and C.-H. Lee, Eds. Berlin: Springer-Verlag, 1985.

[6] K. Meyer, M. Pessot, G. Mourou, R. Grondin, and S. Chamoun, "Subpicosecond photoconductivity overshoot in gallium arsenide observed by electro-ooptic sampling," *Appl. Phys. Lett.*, vol. 53, no. 23, pp. 2254–2256, Dec. 1988.

[7] D. H. Auston, "Impulse response of photoconductors in transmission lines," *IEEE J. Quantum Electron.*, vol. QE-19, pp. 639–648, Apr. 1983.

[8] S N. Chamoun *et al.*, "Theoretical and experimental investigations of subpicosecond photoconductivity," *J Appl. Phys.*, vol. 66, no. 1, pp. 236–246, July 1989.

[9] R. L. Veghte and C. A. Balanis, "Dispersion of transient signals in microstrip transmission lines," *IEEE Trans. Microwave Theory Tech.*, vol. MTT-34, pp. 1427–1436, Dec. 1986.

[10] T. Leung and C. A. Balanis, "Pulse dispersion distortion in open and shielded microstrips using the spectral-domain method," *IEEE Trans. Microwave Theory Tech.*, vol. 36, pp. 1223–1226, July 1988.

[11] M A. Osman and D. K. Ferry, "Electron–hole interaction and high-field transport of photoexcited electrons in GaAs," *J. Appl. Phys.*, vol. 61, pp. 5330–5336, June 1987.

[12] R. Joshi and R O. Grondin, "Hot phonon and electron–hole scattering effects on the transient transport of photogenerated electrons in GaAs," *J. Appl. Phys.*, to be published.

[13] A. E. Iverson and D. L. Smith, "Mathematical modeling of photoconductor transient response," *IEEE Trans. Electron Devices*, vol. ED-34, pp. 2098–2107, Oct. 1987.

[14] R. B. Darling, "Analysis of microwave characteristics of photoconductive IC structures," *J. Lightwave Technol.*, vol. LT-5, pp. 325–339, Mar. 1987.

[15] N. C. Kluksdahl, A. M. Kriman, and D. K. Ferry, "Self-consistent study of the resonant-tunneling diode," *Phys. Rev. B*, vol. 39, no. 11, pp. 7720–7734, Apr. 1989.

[16] A. R. Vasconcelos and R. Luzzi, "Ultrafast transient transport in nonequilibrium semiconductors," *Phys. Rev. B*, vol. 27, no. 6, pp. 3874–3877, Mar. 1983.

[17] J. R. Barker and D. K. Ferry, "On the physics and modeling of small semiconductor devices—I," *Solid-State Electron.*, vol. 23, no. 6, pp. 519–530, June 1980.

[18] R. Grondin and M.-J. Kann, "Transport correlation coefficients and photoconductive switching," *Solid-State Electron.*, vol. 31, nos. 3/4, pp. 567–570, Mar. 1988.

[19] K. Blotekjaer, "Transport equations for electrons in two-valley semiconductors," *IEEE Trans. Electron Devices*, vol. ED-17, pp. 35–47, Jan. 1970.

[20] W. J. R. Hoefer, "The transmission-line matrix method—Theory and applications," *IEEE Trans. Microwave Theory Tech.*, vol. MTT-33, no. 10, pp. 882–893, 1985.

[21] S. Nam, S. El-Ghazaly, H. Ling, and T. Itoh, "Time-domain method of lines," in *1988 IEEE MTT-S Int. Microwave Symp. Dig.*, May 1988, pp. 627–630.
[22] K. S. Yee, "Numerical solution of initial boundary value problems involving Maxwell's equations in isotropic media," *IEEE Trans. Antennas Propagat.*, vol. AP-14, pp. 302–307, 1966.
[23] X. Xhang, J. Fang, K. K. Mei, and Y. Liu, "Calculation of the dispersive characteristics of microstrips by the time-domain finite difference method," *IEEE Trans. Microwave Theory Tech.*, vol. 36, pp. 263–267, Feb. 1988.
[24] X. Zhang and K. K. Mei, "Time-domain finite difference approach to the calculation of the frequency-dependent characteristics of microstrip discontinuities," *IEEE Trans. Microwave Theory Tech.*, vol. 36, pp. 1775–1787, Dec. 1988.
[25] B. Engquist and A. Majda, "Absorbing boundary conditions for the numerical simulation of waves," *Math. Comput.*, vol. 31, no. 139, pp. 629–651, July 1977.
[26] G. Mur, "Absorbing boundary conditions for the finite-difference approximation of the time-domain electromagnetic-field equations," *IEEE Trans. Electromagn. Compat.*, vol. EMC-23, pp. 377–382, Nov. 1981.
[27] V. D. Dymnikov, I. I. Reshina, and V. F. Sapega, "Role of the split-off subband in the polarization of hot photoluminescence of GaAs type semiconductors," *Sov. Phys.—Solid State*, vol. 23, no. 3, pp. 415–419, Mar. 1981.
[28] C. Jacoboni and L. Reggiani, "The Monte Carlo method for the solution of charge transport in semiconductors with application to covalent materials," *Rev. Mod. Phys.*, vol. 55, no. 3, pp. 645–705, July 1983.
[29] M. A. Osman and D. K. Ferry, "Monte Carlo investigation of the electron–hole interaction effects on the ultrafast relaxation of hot photoexcited carriers in GaAs," *Phys. Rev. B*, vol. 36, no. 11, pp. 6018–6032, Oct. 1987.
[30] M. Asche and O. G. Sarbei, "The role of electron–hole interactions in the cooling process of highly excited carriers," *Phys. Status Solidi B*, vol. 126, no. 2, pp. 607–616, Dec. 1984.
[31] R. Joshi and R. O. Grondin, "A self consistent Monte Carlo method for the transient response of laser excited photoconductive circuits," presented at the Sixth Conf. Hot Carriers in Semiconductors, Scottsdale, AZ, July 1989; to be published in *Solid-State Electron*.
[32] Y. Lu, P. Joshi, S. El-Ghazaly, and R. O. Grondin, "Time-domain finite difference and EMC study of hot carrier transport in GaAs on a picosecond scale," presented at 6th Int. Hot Electron Conf., Scottsdale, AZ, July 1989; to be published in *Solid-State Electron*.

✠

Samir M. El-Ghazaly (S'86–M'88) was born in Egypt on July 1, 1959. He received the B.Sc. degree in electronics and communications engineering (distinction, honors) in 1981 and the M.Sc. degree in 1984, both from Cairo University, Cairo, Egypt, and the Ph.D. degree, in electrical engineering, from the University of Texas at Austin in 1988.

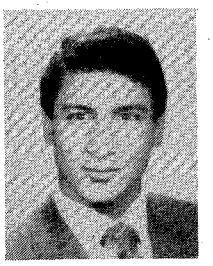

In October 1981 he was appointed as a Teaching Assistant in the Department of Electronics and Communication Engineering, Cairo University, and became Assistant Lecturer there in 1984. From November 1982 to October 1983, he was with the Centre Hyperfrequences et Semiconducteurs, Université de Lille I, Lille, France, where he worked on the simulation of submicronic-gate MESFET's. In January 1984, he joined the Department of Electrical Engineering, University of Ottawa, Canada, where he worked on the analysis of E-plane circuits. In September 1986, he joined the Department of Electrical and Computer Engineering at the University of Texas at Austin as a research assistant and in 1988 became a postdoctoral fellow. In September 1988, he joined Arizona State University, where he is currently an Assistant Professor.

✠

Ravindra P. Joshi received the B. Tech. degree from the Indian Institute of Technology (Bombay) in 1983, the M. Tech. degree from the Indian Institute of Technology (Kanpur) in 1985, and the Ph.D. degree from Arizona State University in 1988, all in electrical engineering. His Ph.D. research involved modeling transient relaxation in photoexcited quantum wells.

He was a postdoctoral fellow at Arizona State University from 1988 to 1989 before joining Old Dominion University in the fall of 1989. His research interests include the physics of ultrafast, nonequilibrium phenomena and Monte Carlo modeling for device applications.

✠

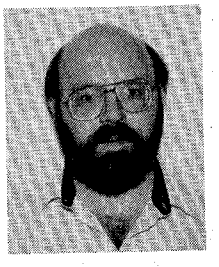

Robert O. Grondin (S'72–M'81–SM'88) was born in 1952 and raised in Michigan. He attended the University of Michigan, receiving the B.S., M.S. and Ph.D. degrees in electrical engineering. In 1981 he bacame a postdoctoral research fellow in the Department of Electrical Engineering at Colorado State University.

In 1983 he joined the faculty of the Department of Electrical and Computer Engineering at Arizona State University, where he presently is an Associate Professor. Dr. Grondin was named a Presidential Young Investigator by the National Science Foundation in 1985.